Oscillatory Tracking of Continuous Attractor Neural Networks Account for Phase Precession and Procession of Hippocampal Place Cells – Supplementary Information

Anonymous Author(s)
Affiliation
Address
email

This supplementary document summarizes the parameter configurations for producing figures in the main text as well as the detailed mathematical derivations. You can also run the matlab code in the zip file if you are interested in the detailed implementation. It is organized as follows:

- Sec.1 summarizes all the parameters that we used in the simulation shown in the main text.
- Sec.2 shows the analytical derivation of the intrisic mobility of our model.
- Sec.3 shows the detailed mathematical analysis of the oscillatory tracking state.
- Sec.4 presents the details for the comparison between our simulation results and the adapted experimental data from [1] and [2].

We also include two videos showing how the oscillatory tracking state naturally give rise to the bursting activities of bimodal cells and unimodal cells at the single neuron level.

1 Parameter configurations

Parameters that are fixed across all simulations are given in Table.1. For validating different aspects of oscillatory tracking, we tune the external input strength α and the feedback inhibition strength m, and the values are summarized in Table. 2.

Table 1: Values for common parameters in all figures

number of neurons: N	512
recurrent connection range: a	0.4
time constant of $U(x,t)$: τ (ms)	3
time constant of $V(x,t)$: τ_v (ms)	144
gain factor: g	5
recurrent connection strength: J_0	0.2
moving speed of the external input: v_{ext} (m/s)	1.45

Submitted to 36th Conference on Neural Information Processing Systems (NeurIPS 2022). Do not distribute.

Table 2: Values for figure specific parameters

Figures \ Parameters	α	m	k
Fig 2B	0	(0,0.12)	0.7
Fig 2D, 2E, 2F	0.1	0.3125, 0.1250, 0.21	0.7
Fig 2C, 3B, 3C	(0.14,0.35)	(1.7, 4.2)	5
Fig 4B, 4C	0.19	2.3	5
Fig 3A, 4A, 5B 5C upper panel	0.19	3.125	5
Fig 5B, 5C lower panel	0.19	3.15	5

2 Analytical derivation of the intrinsic mobility of the CANN

2.1 The network model and dynamic simplification by the projection method

For the convenience of reading, we write down again the network dynamics here (for the detailed description of each variable, see the main text.):

$$\tau \frac{dU(x,t)}{dt} = -U(x,t) + \rho \int_{-\infty}^{\infty} J(x,x')r(x',t)\,dx' - V(x,t) + I^{ext}(x,t), \tag{1}$$

$$\tau_v \frac{dV(x,t)}{dt} = -V(x,t) + mU(x,t), \tag{2}$$

$$r(x,t) = \frac{U(x,t)^2}{1 + k\rho \int_{-\infty}^{\infty} U(x',t)\,dx'}. \tag{3}$$

The connection profile between neurons is set to be,

$$J(x,x') = \frac{J_0}{2\pi a} \exp\left[-\frac{(x-x')^2}{2a^2}\right], \tag{4}$$

It is known that without the external input and feedback inhibition ($\alpha = 0$,$m = 0$), the vanilla CANN holds a continuous family of Gaussian-shaped (bump-like) stationary states when $k < \rho J_0^2/(8\sqrt{2\pi}a)$ (see 2.2 for the derivation). These bump states are expressed as $\overline{U}(x) = A_U \exp\left[-(x-z)^2/(4a^2)\right]$, with z a free parameter and A_U a constant [3].

According to the simulations, we observed that, when both of the external input and negative feedback are applied, the network bump state can still be well approximated with the Gaussian-like profile, which is written as

$$\overline{U}(x,t) = A_u \exp\left\{-\frac{[x-z(t)]^2}{4a^2}\right\}, \tag{5}$$

$$\overline{V}(x,t) = A_v \exp\left\{-\frac{[x-z(t)+d(t)]^2}{4a^2}\right\}, \tag{6}$$

$$\overline{r}(x,t) = A_r \exp\left\{-\frac{[x-z(t)]^2}{2a^2}\right\}, \tag{7}$$

where A_u, A_v and A_r represent the heights of neural bumps. $z(t)$ is the center of $U(x,t)$ and $r(x,t)$, and $d(t)$ denotes the displacement between $U(x,t)$ and $V(x,t)$, and $d(t) > 0$ always holds, as the negative feedback is delayed. To simplify the analysis, we assume that the bump heights, i.e. A_u, A_v and A_r, are all constants.

Substituting Eqs.(5,6,7) into the network dynamics described in Eqs.(1,2,3), we obtain

$$A_r = \frac{A_u^2}{1+k\rho\sqrt{2\pi}aA_u^2}, \tag{8}$$

$$\tau\left[A_u\frac{x-z}{2a^2}\frac{dz}{dt}+\frac{dA_u}{dt}\right]\mathcal{N}(z,2a) = (-A_u+\frac{\rho J_0}{\sqrt{2}}A_r)\mathcal{N}(z,2a) - A_v\mathcal{N}(z-d,2a)+I^{ext}(x,t), \tag{9}$$

$$\tau_v\left[A_v\frac{x-z+d}{2a^2}\frac{d(z-d)}{dt}+\frac{dA_v}{dt}\right]\mathcal{N}(z-d,2a) = -A_v\mathcal{N}(z-d,2a) + mA_u\mathcal{N}(z,2a), \tag{10}$$

with $\mathcal{N}(z,2a)=exp\left\{-\left[x-z\right]^2/4a^2\right\}$.

As a consequence of the translation-invariant connections between neurons, an important property of the CANN is that its dynamics is dominated by a few motion modes [3]. We can therefore simplify the network dynamics significantly by projecting it onto the dominating motion modes (projecting a function $f(x)$ onto a mode $u_n(x)$ means computing $\int_x f(x)u_n(x)dx$). The two most dominant motion modes in the CANN are the bump height and the bump location, and projecting onto these two motions modes is adequate to approximate the network dynamics. For the bump $U(x,t)$, the first two motion modes are,

$$u_0(x,t) = \exp\left\{-\frac{[x-z(t)]^2}{4a^2}\right\}, \tag{11}$$

$$u_1(x,t) = [x-z(t)]\exp\left\{-\frac{[x-z(t)]^2}{4a^2}\right\}. \tag{12}$$

For the bump $V(x,t)$, the first two motion modes are,

$$v_0(x,t) = \exp\left\{-\frac{[x-z(t)+d(t)]^2}{4a^2}\right\}, \tag{13}$$

$$v_1(x,t) = [x-z(t)+d(t)]\exp\left\{-\frac{[x-z(t)+d(t)]^2}{4a^2}\right\}. \tag{14}$$

2.2 Deriving the condition of generating static bump state when $I^{ext}(x,t)=0$

We first consider the simplest case that there is no external drive, and the feedback inhibition is too weak to generating traveling wave state. We are interested in that, under which case the network state can hold a Gaussian-like bump profile as its stationary state. In such a case, we have $dz/dt=0$ and $d=0$, as the bump is static over time. Therefore Eqs. (9-10) are simplified as,

$$\tau\frac{dA_u}{dt} = -A_u+\frac{\rho J_0}{\sqrt{2}}A_r-A_v, \tag{15}$$

$$\tau_v\frac{dA_v}{dt} = -A_v+mA_u. \tag{16}$$

Combining with Eq.(8), we get an active steady state of the network, which is given by,

$$A_v = mA_u, \tag{17}$$

$$A_r = \frac{\sqrt{2}(1+m)}{\rho J_0}A_u, \tag{18}$$

$$A_u = \frac{\rho J_0+\sqrt{\rho^2J_0^2-8\sqrt{2\pi}(1+m)^2k\rho a}}{4\sqrt{\pi}(1+m)k\rho a}. \tag{19}$$

To analyze the stability of this solution, we calculate the Jacobian matrix given by eqn. (17-19), which is given by,

$$\mathbf{M}=\begin{pmatrix} \frac{1}{\tau}\left(-1+\frac{\rho J_0A_u}{1+2\sqrt{\pi}k\rho aA_u^2}\right) & -\frac{1}{\tau} \\ \frac{m}{\tau_v} & -\frac{1}{\tau_v}\end{pmatrix}. \tag{20}$$

Denote the eigenvalues of the Jacobian matrix as λ_1 and λ_2. The condition for the solution to be stable is that both eigenvalues are negative, which is equivalent to,

$$\lambda_1 + \lambda_2 = \frac{1}{2}\left[-1 + \frac{A_u J_0 \rho}{1 + 2\sqrt{\pi} a k \rho A_u^2} - \frac{\tau}{\tau_v}\right] < 0, \tag{21}$$

$$\lambda_1 \lambda_2 = \frac{\tau}{\tau_v}\left(m + 1 - \frac{A_u J_0 \rho}{1 + 2\sqrt{\pi} a k \rho A_u^2}\right) > 0. \tag{22}$$

The above inequalities are satisfied when,

$$0 < k < k_{c1} = \frac{\rho J_0^2 (1 + \frac{\tau}{\tau_v})(1 + 2m - \frac{\tau}{\tau_v})}{8\sqrt{2\pi} a (1+m)^4}, \tag{23}$$

$$0 < k < k_{c2} = \frac{\rho J_0^2}{8\sqrt{2\pi} a (1+m)^2}. \tag{24}$$

It is easy to check that $k_{c2} < k_{c1}$, so the condition for the network to hold static bumps is $0 < k < k_{c2}$.

2.3 Deriving the condition of generating travelling wave state when $I^{ext}(x,t) = 0$

We further derive the condition for the network to hold a travelling wave state, i.e., the network bump moves spontaneously on the neuronal track. We will focus on the feedback inhibition strength m here, as this parameter directly affect the bump mobility. In the travelling wave state, the bump will move at a constant speed and its position is expressed as,

$$z(t) = v_{int} t, \tag{25}$$

where v_{int} is the intrinsic speed of the network bump. Since the bump height is unchanged and the displacement d is a constant in the travelling wave state, Eqs. (9-10) can be simplified as,

$$\tau\left(A_u \frac{x - z}{2a^2} v_{int}\right)\mathcal{N}(z, 2a) = (-A_u + \frac{\rho J_0}{\sqrt{2}} A_r)\mathcal{N}(z, 2a) - A_v \mathcal{N}(z - d, 2a) \tag{26}$$

$$\tau_v\left(A_v \frac{x - z + d}{2a^2} v_{int}\right)\mathcal{N}(z - d, 2a) = -A_v \mathcal{N}(z - d, 2a) + m A_u \mathcal{N}(z, 2a). \tag{27}$$

Projecting both sides of Eq. (26) onto the motion mode $u_0(x)$ (given by Eq.11), we obtain

$$\begin{aligned} Left - side &= 0, \\ Right - side &= (-A_u + \frac{\rho J_0}{\sqrt{2}} A_r)\sqrt{2\pi} a - A_v \exp(-\frac{d^2}{8a^2})\sqrt{2\pi} a. \end{aligned}$$

Equating both sides, we have

$$-A_u + \frac{\rho J_0}{\sqrt{2}} A_r - A_v \exp(-\frac{d^2}{8a^2}) = 0. \tag{28}$$

Similarly, projecting Eq. (26) onto the motion mode $u_1(x)$ (given by Eq.12) and equating both sides, we obtain

$$\tau A_u v_{int} = d A_v \exp(-\frac{d^2}{8a^2}). \tag{29}$$

Again, projecting both sides of Eq. (27) onto the motion modes $u_0(x)$ and $v_1(x)$, respectively, and equating both sides, we obtain

$$\frac{d}{4a^2}\tau_v A_v \exp(-\frac{d^2}{8a^2}) v_{int} = -A_v \exp(-\frac{d^2}{8a^2}) + m A_u, \tag{30}$$

$$\tau_v (1 - \frac{d^2}{4a^2}) v_{int} = d. \tag{31}$$

Combining 8,28-31, we obtain ,

$$A_u = \frac{\rho J_0 + \sqrt{\rho^2 J_0^2 - 8\sqrt{2\pi}k\rho a(1+\sqrt{\frac{m\tau}{\tau_v}})^2}}{4\sqrt{\pi}k\rho a(1+\sqrt{\frac{m\tau}{\tau_v}})}, \tag{32}$$

$$A_v = \frac{\rho J_0 + \sqrt{\rho^2 J_0^2 - 8\sqrt{2\pi}k\rho a(1+\sqrt{\frac{m\tau}{\tau_v}})^2}}{2\sqrt{2\pi}k\rho^2 a J_0}, \tag{33}$$

$$A_r = \sqrt{\frac{m\tau}{\tau_v}} \exp\left[\frac{1-\sqrt{\frac{\tau}{m\tau_v}}}{2}\right] \frac{\rho J_0 + \sqrt{\rho^2 J_0^2 - 8\sqrt{2\pi}k\rho a(1+\sqrt{\frac{m\tau}{\tau_v}})^2}}{4\sqrt{\pi}k\rho a(1+\sqrt{\frac{m\tau}{\tau_v}})}, \tag{34}$$

$$d = 2a\sqrt{1-\sqrt{\frac{\tau}{m\tau_v}}}, \tag{35}$$

$$v_{int} = \frac{2a}{\tau_v}\sqrt{\frac{m\tau_v}{\tau} - \sqrt{\frac{m\tau_v}{\tau}}}. \tag{36}$$

It is straightforward to check from Eq. (36) that for $v_{int} > 0$, i.e., the bump has intrinsic mobility, we have

$$m > \frac{\tau}{\tau_v}. \tag{37}$$

3 Analytical derivation of the oscillatory tracking state

We analyze the tracking behaviors of the network in response to an external moving input, with the latter given by,

$$I^{ext} = \alpha \exp\left[-\frac{(x-v_{ext}t)^2}{4a^2}\right], \tag{38}$$

where v_{ext} represents the moving speed of the external input and α the input strength.

The tracking behaviors of the network are determined by two competing factors: one is the intrinsic mobility of the network caused by the feedback inhibition, which tends to drive the bump to move spontaneously (see above derivation); the other is extrinsic mobility caused by the external moving input, which tends to drive the bump to move at the speed v_{ext}. The competition between two factors leads to three tracking states of the network: travelling wave, oscillatory tracking, and smooth tracking. Here we only focus on the analytical derivation of the oscillatory tracking. Based on simulation results, we assume that the bump position is expressed as,

$$z(t) = c_0 sin(\omega t) + d_0 + v_{ext}t, \tag{39}$$

where c_0 and ω represent the amplitude and frequency of the bump position oscillation, respectively, and d_0 denotes the offset between the baseline of bump oscillation and the position of the external input. Substitute the form of external input written in eqn. (38) into eqs. (9-10), we obtain

$$\tau\left(A_u\frac{x-z}{2a^2}\frac{dz}{dt}\right)\mathcal{N}(z,2a) = (-A_u + \frac{\rho J_0}{\sqrt{2}}A_r)\mathcal{N}(z,2a) - A_v\mathcal{N}(z-d,2a) + \alpha\mathcal{N}(v_{ext}t,2a), \tag{40}$$

$$\tau_v\left(A_v\frac{x-z+d}{2a^2}\frac{d(z-d)}{dt}\right)\mathcal{N}(z-d,2a) = -A_v\mathcal{N}(z-d,2a) + mA_u\mathcal{N}(z,2a). \tag{41}$$

Projecting Eq. (40) onto u_0 and u_1, respectively, we get,

$$-A_u + \frac{\rho J_0}{\sqrt{2}}A_r + \alpha\exp(-\frac{s^2}{8a^2}) = A_v\exp(-\frac{d^2}{8a^2}), \tag{42}$$

$$dA_v\exp(-\frac{d^2}{8a^2}) - \alpha\exp(-\frac{s^2}{8a^2}) = \tau A_u\frac{dz}{dt}, \tag{43}$$

where $s(t) = c_0 \sin(\omega t) + d_0$ denotes the offset between $U(x,t)$ and $I_{ext}(x,t)$. For clearance, we denote $A_{temp} = A_v \exp(-d^2/8a^2)$ hereafter.

Substituting Eqs. (39&42) into (43), we obtain

$$d(t) = \frac{1}{A_{temp}} \left[\tau A_u (v + c_0 \omega \cos \omega t) + \alpha s \exp(-\frac{s^2}{8a^2}) \right].$$

Since $s \ll 2a$ generally holds, we consider the approximation of $\exp(-s^2/8a^2) \approx 1$. With this approximation, the above equation can be re-written as

$$d(t) = A_0 \sin(\omega t + \beta) + B_0, \tag{44}$$

where the parameters are,

$$\beta = \arccos\left(\frac{\alpha}{\sqrt{\tau^2 A_u^2 \omega^2 + \alpha^2}} \right), \tag{45}$$

$$A_0 = \frac{c_0 \sqrt{\tau^2 A_u^2 \omega^2 + \alpha^2}}{A_{temp}}, \tag{46}$$

$$B_0 = \frac{\tau A_u v + \alpha d_0}{A_{temp}}. \tag{47}$$

Similarly, projecting Eq. (41) onto v_0 and v_1, respectively, we obtain,

$$A_v = m A_u \exp(-\frac{d^2}{8a^2}), \tag{48}$$

$$\tau_v A_v \left[\frac{\mathrm{d}z(t)}{\mathrm{d}t} - \frac{\mathrm{d}d(t)}{\mathrm{d}t} \right] = m A_u \exp(-\frac{d^2}{8a^2}) d(t). \tag{49}$$

Substituting Eqs. (8 & 48) into (42), we have

$$-A_u + \frac{\rho J_0}{\sqrt{2}} \frac{A_u^2}{1 + \sqrt{2\pi} ak\rho A_u^2} + \alpha \exp(-\frac{s^2}{8a^2}) = m A_u \exp(-\frac{d^2}{4a^2}).$$

Since $s \ll 2a$ and $d \ll 2a$, the approximations $\exp(-s^2/8a^2) \approx 1$ and $\exp(-d^2/4a^2) \approx 1$ hold, and the above equation can be simplified as,

$$(m+1) A_u - \frac{\rho J_0}{\sqrt{2}} \frac{A_u^2}{1 + \sqrt{2\pi} ak\rho A_u^2} - \alpha = 0.$$

We note that $\sqrt{2\pi} ak\rho A_u^2 \gg 1$ when the network is at the oscillatory tracking state, which gives $A_u^2/(1 + \sqrt{2\pi} ak\rho A_u^2) \approx 1/\sqrt{2\pi} ak\rho$. Thus, we have

$$A_u = \frac{J_0 + 2\sqrt{\pi} ak\alpha}{2\sqrt{\pi} ak(1+m)}. \tag{50}$$

Substituting Eq. (48) into (49), we have

$$\tau_v \frac{\mathrm{d}z(t)}{\mathrm{d}t} = d(t) + \tau_v \frac{\mathrm{d}d(t)}{\mathrm{d}t}. \tag{51}$$

Substituting Eqs. (39 & 44) into (51), we have

$$\tau_v (v + c_0 \omega \cos \omega t) = A_0 \left[\sin(\omega t + \beta) + \omega \tau_v \cos(\omega t + \beta) \right] + B_0.$$

Using the trigonometric transformation formula, the above equation is re-written as,

$$\tau_v v + \tau_v c_0 \omega \sin(\omega t + \frac{\pi}{2}) = A_0 \sqrt{1 + \omega^2 \tau_v^2} \sin(\omega t + \beta + \gamma) + B_0, \tag{52}$$

where γ is given by

$$\gamma = \arccos(\frac{1}{\sqrt{\tau_v^2 \omega^2}}). \tag{53}$$

Equating two sides of Eq. (52), we have,

$$\begin{aligned} \tau_v v &= B_0, && (54)\\ \frac{\pi}{2} &= \beta + \gamma, && (55)\\ \tau_v c_0 \omega &= A_0\sqrt{1+\omega^2\tau_v^2}. && (56) \end{aligned}$$

Substituting Eq. (47) into (54), we obtain

$$d_0 = \frac{\tau_v v A_{temp} - \tau v A_u}{\alpha}. \tag{57}$$

Applying the cosine function to both sides of Eq. (55), we have

$$\cos(\beta+\gamma) = \cos\gamma\cos\beta - \sin\gamma\sin\beta = 0. \tag{58}$$

Substituting Eqs. (45 & 53) into (58), we have

$$\omega^2 = \frac{\alpha}{\tau\tau_v A_u}. \tag{59}$$

Combining Eq. 59 with Eq. (50), we obtain

$$\omega = \sqrt{\frac{2\sqrt{\pi}\alpha a k(1+m)}{\tau\tau_v(J_0 + 2\sqrt{\pi}ak\alpha)}}. \tag{60}$$

Substituting Eqs. (46 & 59) into (56), and taking square for both sides, we have

$$\frac{(\tau^2 A_u^2\omega^2 + \alpha^2)}{A_{temp}^2}(1+\omega^2\tau_v^2) = \tau_v^2\omega^2.$$

Solving the above equation for A_{temp}, we get

$$A_{temp} = \frac{\tau A_u + \alpha\tau_v}{\tau_v}. \tag{61}$$

Substituting Eq. (61) into (57), we can get the expression for d_0, which is

$$d_0 = \tau_v v. \tag{62}$$

Since $A_{temp} = mA_u \exp\left[-d(t)^2/(4a^2)\right]$ varies across time, we take the approximation

$$A_{temp} = mA_u \exp\left[-\overline{d(t)^2}/(4a^2)\right] \tag{63}$$

with $\overline{d(t)^2}$ the time-averaged value, which is calculated to be,

$$\overline{d(t)^2} = \frac{1}{T}\int_0^T d^2(t)dt = \frac{\alpha\tau_v}{2(\tau A_u + \alpha\tau_v)}c_0^2 + \tau_v^2 v^2. \tag{64}$$

Substituting Eqs. (61 & 64) into (63), we obtain,

$$c_0 = \sqrt{\frac{2\left[4a^2(\ln\frac{\tau_v m A_u}{\tau A_u + \alpha\tau_v}) - \tau_v^2 v^2\right](\tau A_u + \alpha\tau_v)}{\alpha\tau_v}}. \tag{65}$$

Substituting Eq. (61) into (48) and utilizing the condition of $\exp(-d^2/8a^2) = \sqrt{A_{temp}/mA_u}$, we obtain

$$A_v = \sqrt{\frac{\tau A_u + \alpha\tau_v}{\tau_v}}mA_u. \tag{66}$$

Finally, combining Eqs.(8, 50, 62, 60, 65, 66), we get all unknown parameters of the oscillatory tracking state, which are,

$$A_u = \frac{J_0 + 2\sqrt{\pi}ak\alpha}{2\sqrt{\pi}ak(1+m)}, \tag{67}$$

$$A_r = \frac{A_u^2}{1 + \sqrt{2\pi}ak\rho A_u^2}, \tag{68}$$

$$A_v = \sqrt{\frac{\tau A_u + \alpha\tau_v}{\tau_v} m A_u}, \tag{69}$$

$$c_0 = \sqrt{\frac{2\left[4a^2 \ln \frac{\tau_v m A_u}{\tau A_u + \alpha\tau_v} - \frac{\omega}{2\pi}\tau_v^2 v^2\right](\tau A_u + \alpha)}{\alpha\tau_v}}, \tag{70}$$

$$d_0 = \tau_v v, \tag{71}$$

$$\omega = \sqrt{\frac{2\sqrt{\pi}\alpha ak(1+m)}{\tau\tau_v(J_0 + 2\sqrt{\pi}ak\alpha)}}. \tag{72}$$

4 Related experimental results of the theta sequences

4.1 The forward and backward theta sweeps in the experiment

Fig.4A in the main text shows comparison between our simulation results and the experimental results of the decoded virtual position of the neural activities with respect to the rat's position. In the experiment, they decoded the neural activities (spike train) through Bayesian inference by assuming that the place cells fire independently and obey a Poisson statistics [1]. Specifically, they first recorded the mean probability of the neurons firing spikes as a function of space as the rats moved through the maze. For the ith neuron, if denoting $f_i(z)$ as the tuning function, then the number of spikes n_i it generates within a time interval Δt when the animal locates at z satisfies the Poisson distribution, which is expressed as,

$$P(n_i|z) = \frac{[f_i(z)\Delta t]^{n_i}}{n_i!} e^{-f_i(z)\Delta t}, \tag{73}$$

Denote $\mathbf{n} = \{n_i\}$, for $i = 1, \ldots, N$, the numbers of spikes generated by the neuron ensemble within the time interval Δt. Assuming that neurons fire independently, the likelihood function of observing $\mathbf{n}$ when the animal locates at z can be written as

$$P(\mathbf{n}|z) = \prod_{i=1}^{N} P(n_i|z). \tag{74}$$

Assuming the prior distribution of the animal location is uniform (i.e., $P(z)$ is flat), the posterior of the animal location given the spike events is given by

$$\begin{aligned} P(z|\mathbf{n}) &= P(\mathbf{n}|z)P(z), \\ &= C_0 \prod_{i=1}^{N} P(n_i|z), \end{aligned} \tag{75}$$

with C_0 a normalization constant. Fig.1A shows the decoded spatial representation probability $P(z|\mathbf{n})$ relative to the rat's current location (blue line) and movement direction. We can see clearly there exists a positive offset in the sweeps which supports a stronger prospective encoding in the forward theta sequences. Alternating forward and reverse theta sequences were observed in rats when they are exploring an open field or a linear tracks (see fig.1B). This may indicate that place cells in the hippocampus have adopted a spatial coding mode that combines prospective (forward sweeps) and retrospective (backward sweeps) coding.

4.2 Phase shifts of unimodal cells and bimodal cells in the experiment

To compare with the experimental data [1], we follow the experimental protocol to calculate the averaged phase shift effects of each type of cells.

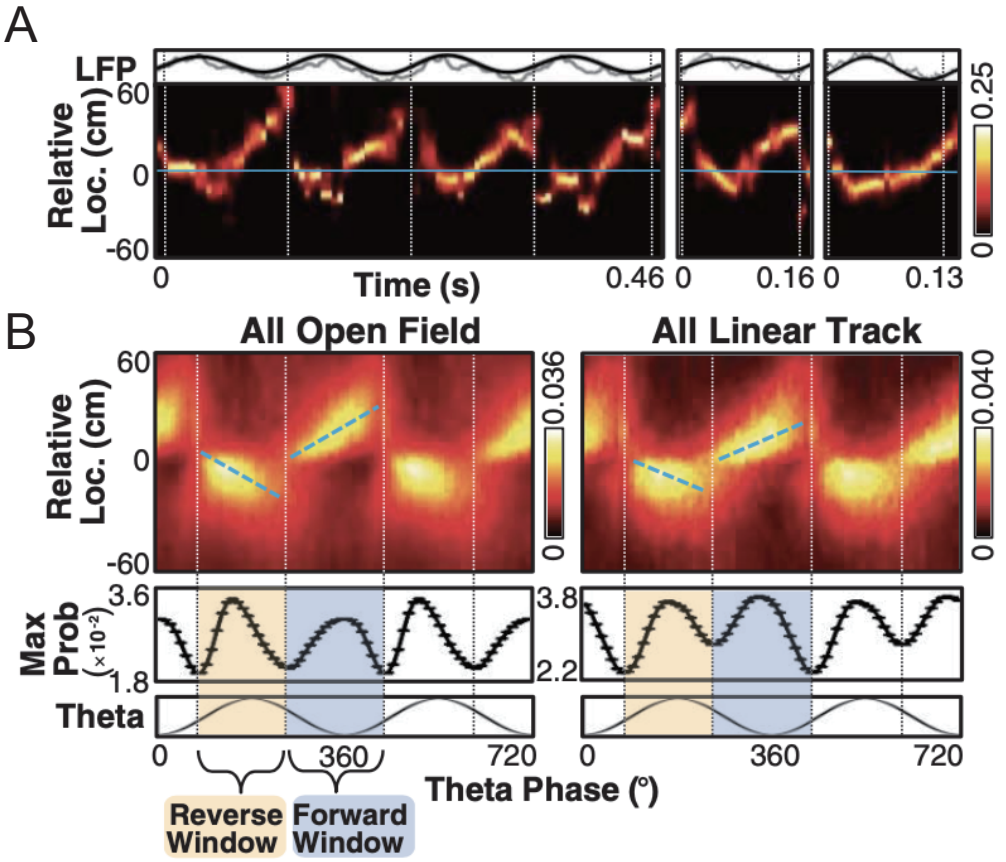

Figure 1: The experimental data shows alternative forward and reverse theta sweeps. A. Decoded relative positions of the place cell activities shows forward and reverse theta sweeps (Single trial). B. Averaged probability distribution (over trials and over theta cycles) of the decoded virtual positions of the place cell activities when the rat is exploring either in an open field (left panel) or in linear tracks (right panel). The experimental data is adapted from [1].

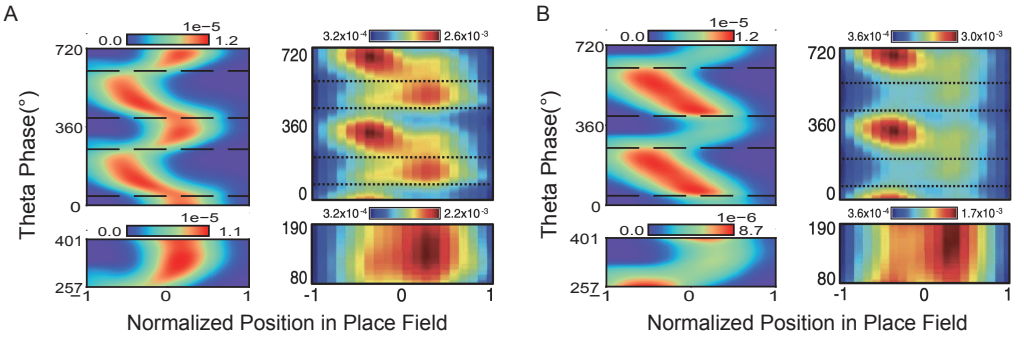

Figure 2: Comparison between our simulation results and the experimental results of the phase shift of unimodal cells and bimodal cells. A. The phase shift of bimodal cells. Left panel: our simulation results. Right panel: experimental data. B. The phase shift of unimodal cells. Left panel: our simulation results. Right panel: experimental data. The parameters are the same as those used in Fig.5 in the main text. The experimental data is adapted from [1].

Firstly, rather than measuring the phase of neuronal firing by using only the response peak as done in the theoretical analysis, we calculate the distribution of neuronal firing phase by using the neuronal response at each moment as the intensity of the corresponding phase (this essentially leads to the same conclusion as in the theoretical analysis, but for the experimental data, since the response peak is vague, the analysis has to be done in such a way). For example, if the neuronal response at the moment Δt in a theta cycle is $r(\Delta t)$, then the firing phase is $\theta = \Delta t/T \times 2\pi$ (note that the moment in a theta cycle is counted from 0 to T) and it occurs with the intensity $r(\Delta t)$. Secondly, we align phase shifts of all bimodal (or unimodal) cells in the network together according to the normalized position of the animal in the place field of each neuron. For example, if the animal is located at $v_{ext}t$ and its displacement to the place field center x_0 of a neuron is $(v_{ext}t - x_0)$, then the normalized position of the animal with respect to this neuron is calculated to be $\tilde{x} = (v_{ext} - x_0)/(2.5a)$, with a the width of the bump. We only consider phase shift for $\tilde{x}$ in the range of $[-1, 1]$, with $\tilde{x} = -1$ corresponding to that the animal just enters the place field of the neuron and $\tilde{x} = 1$ the animal leaves the place field of the neuron. Following the experimental protocol [1], we calculate the phase shift effect summed over bimodal or unimodal cells then normalize the total distribution to make sure that the summation of the joint probability distribution equals 1. For each type of cells, the intensity of phase θ at a normalized position $\tilde{x}$ is then calculated to be

$$P(\theta, \tilde{x}) = C \sum_{i=1}^{N_c} \theta r_i(\Delta t, \tilde{x}), \tag{76}$$

where the relationship $\theta = \Delta t/T \times 2\pi$ holds, and $r_i(\Delta t, \tilde{x})$ denotes the response of the i-th neuron at the moment Δt in a theta cycle when the animal locates at $\tilde{x}$. N_c is the number of neurons of the cell type, and the summation runs over all neurons of the same type. C is the normalized factor. The comparison between our simulation results and the experimental data are shown in Fig. 2. Consistent with our analysis, both unimodal cells and bimodal cells exhibits phase pre- and procession. However, the strength of the phase procession between the two cell types are different. For bimodal cells, because the bump height keeps almost invariant during the forward sweeps and the backward sweeps, both of the phase precession and the phase procession are significant. For unimodal cells, because the bump height attenuates significantly during the backward sweeps, the phase procession is not as significant as the phase precession.

References

[1] Mengni Wang, David J Foster, and Brad E Pfeiffer. Alternating sequences of future and past behavior encoded within hippocampal theta oscillations. Science, 370(6513):247–250, 2020.

[2] William E Skaggs, Bruce L McNaughton, Matthew A Wilson, and Carol A Barnes. Theta phase precession in hippocampal neuronal populations and the compression of temporal sequences. Hippocampus, 6(2):149–172, 1996.

[3] CC Alan Fung, KY Michael Wong, and Si Wu. A moving bump in a continuous manifold: a comprehensive study of the tracking dynamics of continuous attractor neural networks. Neural Computation, 22(3):752–792, 2010.